Available online at www.sciencedirect.com
ScienceDirect
Polymer 48 (2007) 2853–2859
polymer
www.elsevier.com/locate/polymer

Synthesis and characterization of ZnS/hyperbranched polyester nanocomposite and its optical properties

Yongbin Zhao [a,b], Feng Wang [b], Qi Fu [a], Wenfang Shi [a,*]

[a] Department of Polymer Science and Engineering, University of Science and Technology of China, Hefei, Anhui 230026, PR China
[b] Department of carbon nanofiber & composite, College of Materials Science and Technology, Beijing University of Chemical and Technology, Beijing 100029, PR China

Received 17 January 2007; received in revised form 16 March 2007; accepted 17 March 2007
Available online 28 March 2007

Abstract

The ZnS/hyperbranched polyester nanocomposite with higher refractive index was prepared by incorporating the acrylated 2-(2-mercapto-acetoxy)-ethyl ester-capped ZnS nanoparticles into the acrylated Boltorn™ H20 (H20). The acrylated 2-(2-mercapto-acetoxy)-ethyl ester-capped colloidal ZnS nanoparticles were synthesized by the reaction of zinc acetate with thioacetamide in *N*,*N*-dimethylformamide. The acrylated hyperbranched polyester was obtained by reacting acryloyl chloride with hydroxyl group of H20. The acrylated H20 plays an important role in stabilizing and dispersing ZnS nanoparticles with a diameter of 1–4 nm. The refractive indices of ZnS/hyperbranched polyester nanocomposites, depending on ZnS content, were determined to be in the ranges of 1.48–1.65.

Keywords: Hyperbranched polyester; Zinc sulfide; Nanocomposite

1. Introduction

Recently, there has been much interest in the preparation of organic–inorganic hybrid materials with high refractive index because of their potential applications in lenses, optical waveguides, displays and reflectors [1–6]. Two approaches have been developed to prepare organic–inorganic hybrid materials. The first route is to incorporate inorganic domains into a polymer matrix by a sol–gel technique [7,8]. Wilkes and coworkers successfully prepared triethoxysilane-capped polymer–titania hybrid materials, including poly(arylene ether ketone) (PEK) and poly(arylene ether sulfone) (PES). Their refractive indices and the Abbe numbers of PES–TiO_2 and PEK–TiO_2 hybrid materials, depending on TiO_2 content, were in the ranges of 1.60–1.75 and 20–30, respectively [1]. However, the serious shrinkage induced by the drying process limited its application. Another method is to incorporate premade inorganic colloidal nanoparticles into a polymer matrix [9,10]. For instance, the lead sulfide nanoparticles were introduced into poly(ethylene oxide) to produce nanocomposites with higher refractive index [11]. However, the matrices used in these studies are water-soluble polymers and there was no chemical bonding between the nanoparticles and the polymer matrices.

Zinc sulfide (ZnS), due to its high bulk refractive index ($n = 2.36$ at 620 nm by Abbe method) and lack of absorption in the visible and near IR region (from 400 nm to 2400 nm), is an attractive material for the use as a suitable inorganic component to improve the optical properties of nanocomposites. Recently, a novel method has been developed for immobilizing semiconductor nanoparticles into polymer matrices for preparing nanocomposites with high refractive index [12,13]. The nano-ZnS/polythiourethane (PTU) composite films have been prepared via immobilization of thiophenol/mercaptoethanol-capped ZnS nanoparticles with a diameter of 2–6 nm into PTU matrix [14].

Up to now, traditional linear polymers such as MMA, PTU, etc. were often chosen as polymer matrices. The hyperbranched polymers are characterized by their spherical

* Corresponding author. Tel.: +86 551 3606084; fax: +86 551 3606630.
E-mail address: wfshi@ustc.edu (W. Shi).

0032-3861/$ - see front matter © 2007 Elsevier Ltd. All rights reserved.
doi:10.1016/j.polymer.2007.03.054

molecular shape and large amount of functional end groups at the molecular surface, which are modified easily for various end-user purposes with different reaction routes [15–17]. Moreover, several intriguing properties such as high reactivity, good compatibility with other materials, high solubility and low viscosity at melt and solution compared with their linear counterparts have been described [18,19]. The difference in chemical and physical properties of hyperbranched polymers to their linear counterparts leads to variation in their morphologies, thermal and mechanical properties of prepared hybrid materials [20–22]. In this work, in order to disperse ZnS nanoparticles in the polymer matrix, the hyperbranched polyester was chosen as a polymer matrix. Moreover, ZnS nanoparticles were prepared by reacting Zn^{2+} ions with S^{2-} ions decomposed by thioacetamide in order to avoid the pollution of H_2S gas used by traditional preparation method.

Therefore, a novel ZnS/hyperbranched polyester nanocomposite with high refractive index was prepared. Firstly, the acrylated 2-(2-mercapto-acetoxy)-ethyl ester-capped colloidal ZnS nanoparticles with narrow size distribution were synthesized by the reaction of zinc acetate with thioacetamide in *N*,*N*-dimethylformamide solution. Secondly, the thiol-capped colloidal ZnS nanoparticles were immobilized into the acrylated hyperbranched polyester through spin-coating and ultraviolet radiation initiated free radical polymerization. A series of ZnS/hyperbranched polyester composites with different ZnS contents were synthesized. The structural characters of thiol-capped ZnS nanoparticles were confirmed by TEM, XRD, and FTIR. The resulting composite film was characterized by TEM and AFM observation and UV–vis spectroscopy. The refractive index was measured at the wavelength of 632.8 nm by an ellipometer.

2. Experimental

2.1. Materials

Hyperbranched polyester, Boltorn™ H20 (H20) (shown in Fig. 1), theoretically having 16 hydroxyl end groups per molecule and the average molecular weight of 1735 g mol^{-1}, was supplied by Perstorp AB, Sweden. Anhydrous zinc acetate, thioacetamide (TAA), thioglycolic acid, dicyclohexyl carbodiimide (DCC), 4-dimethylaminopyridine (DMAP), Darocur 1173 and other chemical reagents (analytical reagent quality) were purchased from China Medicine (Group) Shanghai Chemical Reagent Corporation and used without further purification except 2-hydroxyethyl acrylate (HEA) and acrylic acid (AA), which were freshly vacuum distilled before use. Acryloyl chloride was synthesized in our lab by the reaction of acrylic acid with benzyl chloride.

2.2. Synthesis

2.2.1. Acrylated 2-(2-mercapto-acetoxy)-ethyl ester (AMAEE)

AMAEE was synthesized through the reaction of HEA and thioglycolic acid using DCC and DMAP as catalysts [23]. In a typical synthesis, the solution of HEA (0.05 mol), thioglycolic acid (0.05 mol), DCC (0.055 mol) and DMAP (0.005 mol) in dichloromethane (50 ml) was stirred mechanically at room temperature until the esterification was completed. The resulted byproduct *N*,*N*-dicyclohexylurea was filtered off and the filtrate was washed with water, and then dried over anhydrous sodium sulphate. The solvent was evaporated under reduced pressure, yielding a viscous liquid, named AMAEE (shown as follow).

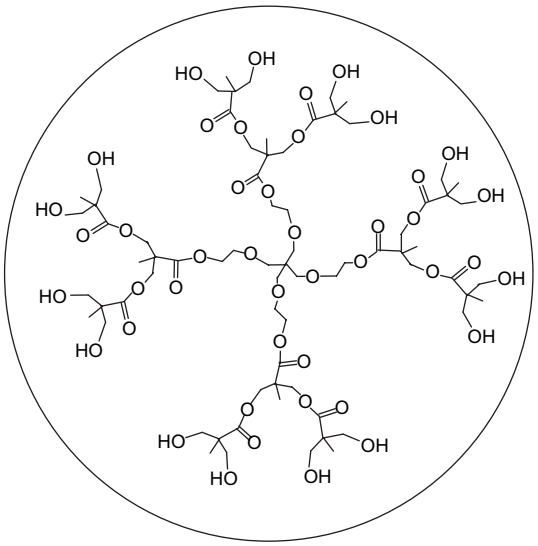

Fig. 1. Ideal molecular structure of Boltorn™ H20.

Formula: $SHCH_2COOCH_2CH_2OOCCH{=}CH_2$; Fw: 190.25.

^1H NMR ($CDCl_3$, ppm): 6.06, 5.48, 5.25 ($-CH{=}CH_2$), 3.55–4.23 ($-C-CH_2-O$), 3.12 ($-CH_2-C{=}O$), 1.53 ($-SH$).

2.2.2. Colloidal ZnS nanoparticles

The thiol-capped ZnS nanoparticles were prepared through the reaction of zinc acetate with sulfur ion from the decomposition of TAA in *N*,*N*-dimethylformamide (DMF). In a typical synthesis, 2.195 g zinc acetate and 1.125 g TAA were dissolved into 50 ml of DMF solution containing 0.76 g AMAEE, and stirred at 80 °C for 3 h. The powder sample for the FTIR measurement was obtained by drying the ZnS–DMF colloidal solution under vacuum.

2.2.3. Acrylated hyperbranched polyester (AH20)

The acrylated H20 (AH20) was acquired by acryloyl chloride as an end-group modifier for etherifying hydroxyl group of H20 [24]. In a typical synthesis, 15.1 g H20 was dissolved in a mixture of dichloromethane (50 ml) and triethylamine (20 ml) with DMAP (0.4 g) as a catalyst, and then added dropwise to an ice-cooled reaction vessel containing 15 ml of acryloyl chloride. The reactants were stirred at room temperature until the hydroxyl peak at 3400–3100 cm^{-1} in the FTIR spectrum disappeared, followed by extraction with HCl (2 M) and $NaHCO_3$ aqueous solution to remove excessive triethylamine, dried over $MgSO_4$ and filtered. Finally, dichloromethane was evaporated, yielding a highly viscous yellowish resin that is denoted as AH20.

^{1}H NMR ($CDCl_3$, ppm): 6.06, 5.48, 5.25 (−C*H*=CH_2), 4.21 (−CH_2−O−CO−), 3.56 (CH_2 of core moiety), 1.117 (−CH_3, bis-MPA).

2.3. Preparation of ZnS/AH20 nanocomposite film

The AH20−DMF solution of desired weight ratio containing 3 wt% of Darocur 1173 as an initiator was mixed with the thiol-capped colloidal ZnS−DMF solution according to the required doping content of ZnS particle in the final cured film. The solution was concentrated to a suitable viscosity at room temperature under vacuum, and then spin-coated on a quartz plate at 1000−3000 rpm. The coated film was dried under vacuum for 10 min at 50 °C, and then exposed to a medium pressure mercury lamp (80 W/cm, Lantian lamp Co., Beijing) to form a film with the thickness of 1 μm.

2.4. Characterization

The transmission electron microscopic (TEM) studies were carried out on a Hitachi Model H-800 (Japan) apparatus with an accelerating voltage of 200 kV. The phase composition and nature of the obtained products were determined by X-ray diffraction (XRD) measurement, using a Rigaku (Japan) D/Max-γA X-ray diffractometer equipped with graphite monochromatized high-intensity Cu Kα radiation (λ = 1.54178 Å). The accelerating voltage was set at 40 kV with a 100 mA flux. The scanning rate was 0.06°/s in the 2θ range of 10°−70°. The FTIR spectra were recorded with a Magna-IR 750 Fourier transform infrared (FTIR) spectrometer using a KBr method. The absorption spectra were examined on a UV-2100 Shimadzu UV−vis spectrophotometer.

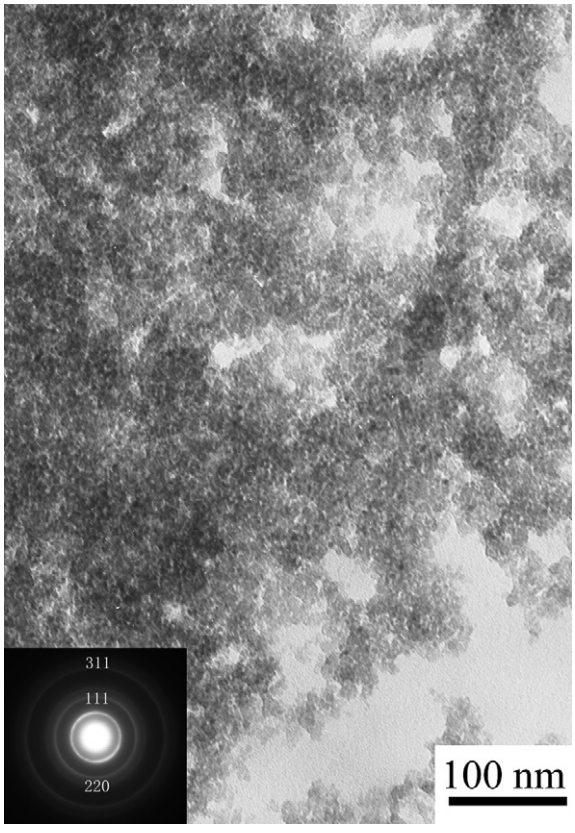

Fig. 2. TEM image and electron diffraction pattern of AMAEE-capped ZnS nanoparticles.

3. Results and discussion

3.1. Structural characteristics

Fig. 2 shows the TEM image and the electron diffraction (ED) pattern of AMAEE-capped ZnS nanoparticles. The small aggregates of nanoparticles are observed from the TEM image. The ZnS nanoparticle has a diameter of about 1−4 nm. In the electron diffraction pattern of ZnS nanoparticles, the

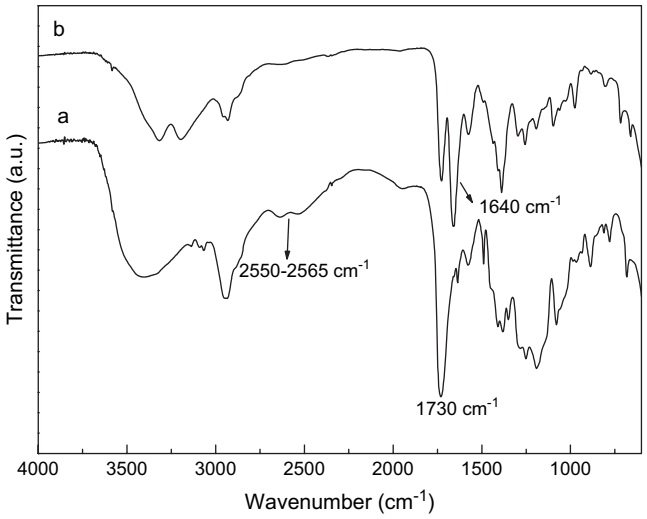

Fig. 3. FTIR spectra of (a) AMAEE and (b) AMAEE-capped ZnS nanoparticles.

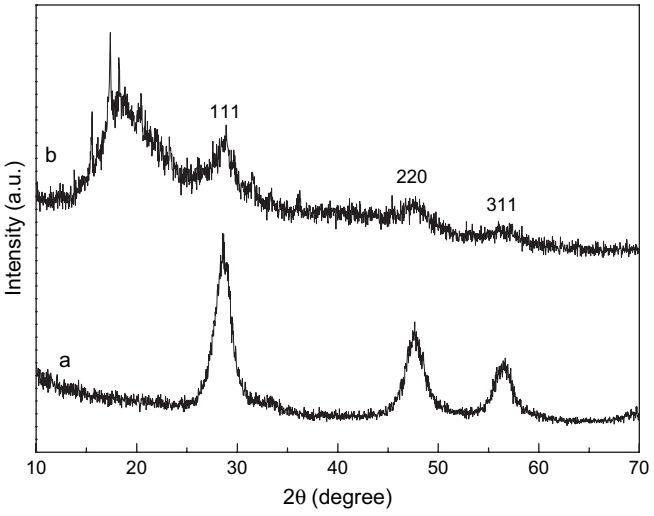

Fig. 4. XRD patterns of (a) AMAEE-capped ZnS nanoparticles and (b) ZnS/AH20 nanocomposites.

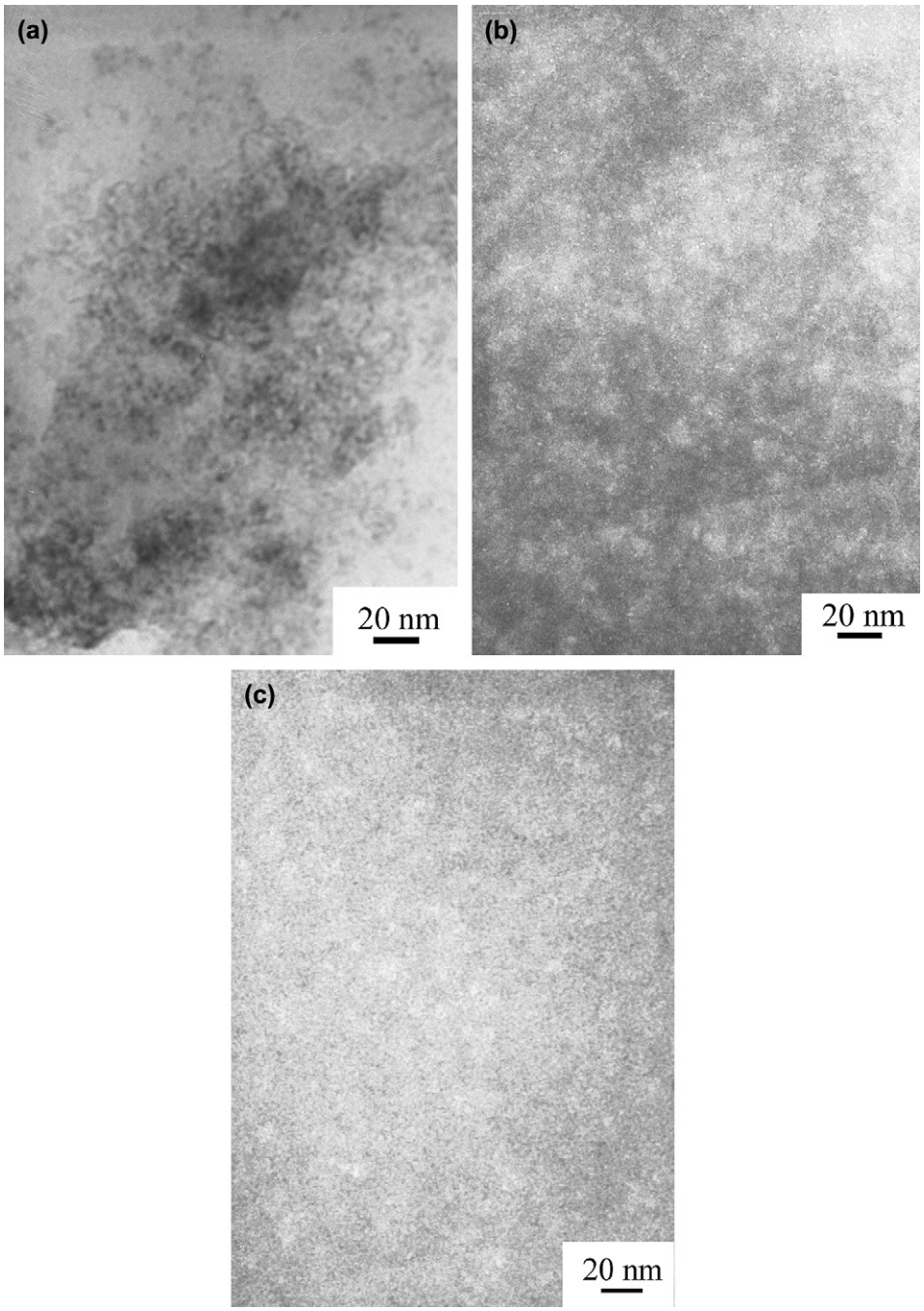

Fig. 5. TEM images of ZnS/AH20 nanocomposite films with ZnS contents of (a) 10 wt%, (b) 20 wt%, and (c) 30 wt%.

apparent diffraction rings assigned to (111), (220) and (311) planes of cubic ZnS crystallite are observed [25].

The FTIR spectra of AMAEE and AMAEE-capped ZnS nanoparticles are shown in Fig. 3. From the IR spectrum as shown as curve (a) in Fig. 3, the peaks at 1730 cm^{-1} for C═O group and at 1640 cm^{-1} for C═C group, and the absorption peak of S–H vibration at 2550–2565 cm^{-1} are observed apparently, indicating the formation of AMAEE. However, the absorption peak of S–H vibration at 2550–2565 cm^{-1} disappeared for AMAEE-capped ZnS nanoparticles, as shown as the curve (b) in Fig. 3, indicating that the thiol groups in AMAEE molecules have been completely bound to the surface of ZnS nanoparticles [26].

The X-ray powder diffraction (XRD) analysis was used to determine the phases of AMAEE-capped ZnS nanoparticles and ZnS/AH20 nanocomposite, as shown in Fig. 4. Zinc sulfide has zinc blended crystal structure according to all the peaks of curve (a). The lattice parameter (a) is 5.405 Å, which is consistent with the reported value of 5.406 Å (JCPDS Card File No. 05-0566). Three diffraction peaks correspond to the (111), (220), and (311) planes of cubic crystalline ZnS, which is in good agreement with the ED information. An average

crystallite size was estimated as about 2.7 nm, according to the line width analysis of the (111) diffraction peak based on Debye–Scherrer formula. The rising background in the lower angle side ($2\theta \approx 20°$) is observed in the curve (b) in Fig. 4, indicating the presence of AH20.

Fig. 5 presents the typical TEM images of ZnS/AH20 nanocomposite films with ZnS contents of 10 wt%, 20 wt%, and 30 wt%. It can be seen from Fig. 5(a) that the ZnS nanoparticles ranging from 1 nm to 4 nm are uniformly dispersed in the polymeric matrix because of lower ZnS content in the nanocomposite film; however, with increasing the ZnS content of 20 wt% and 30 wt% in the nanocomposite film, as shown in Fig. 5(b) and (c), the ZnS nanoparticles are still uniformly dispersed and remain their original size without aggregation after immobilization into the polymer matrix, indicating that both thiol capping agent and hyperbranched polyester play an important role in stabilizing and dispersing nanoparticles.

The AFM images of films without and with ZnS nanoparticles of 15 wt% are shown in Fig. 6. It can be seen that the surface of the film is very flat; however, many small nanoparticles are uniformly dispersed at the surface of nanocomposite film, shown in Fig. 6(b), and the size of ZnS nanoparticles is around 1–4 nm. This further indicates that the ZnS nanoparticles remain their original size without aggregation at the surface of films.

Plotted in Fig. 7 are FTIR spectra of pure AH20 and ZnS/AH20 nanocomposite films with ZnS contents of 10 wt% and 20 wt%. The characteristic peaks at 2855–2933 cm^{-1}, 1733 cm^{-1} and 1162 cm^{-1} in the IR spectrum of the obtained powder are assigned to C–H, ester C=O and C–O groups, respectively, in AMAEE and AH20 can be observed. In addition, the peaks at 1640 cm^{-1} and 810 cm^{-1} for acrylate group disappeared in Fig. 7(b) and (c), indicating that the polymerization has been completely finished.

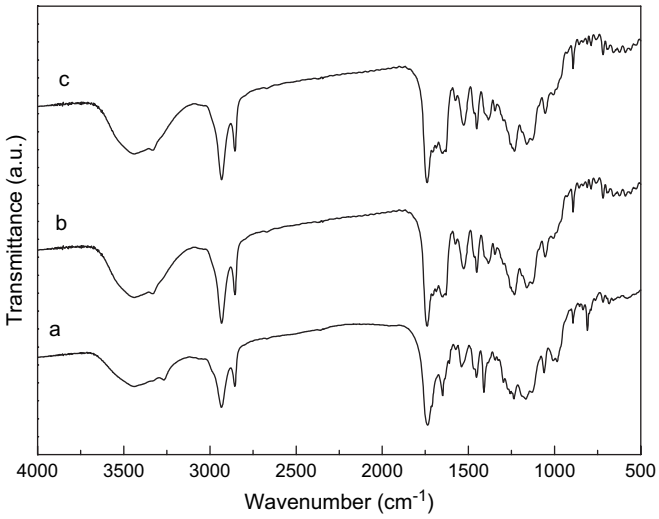

Fig. 7. FTIR spectra of (a) AH20, and ZnS/AH20 nanocomposite films with ZnS contents of (b) 10 wt% and (c) 20 wt%.

3.2. Thermodynamic properties

Fig. 8 presents the thermogravimetric analysis (TGA) results for ZnS/AH20 nanocomposite films with ZnS contents of 5 wt%, 10 wt%, 15 wt%, and 20 wt%. The weight loss of almost 20–30% for all samples is observed from the TGA spectra up to 200 °C, due to the evaporation of residual moisture or solvent adsorbed to the surface or inner of the samples. And then, there are bigger weight losses for all samples with increasing the temperature from 200 °C to 750 °C due to the decomposition of hyperbranched polyester. Whereas, after 750 °C, the weight of samples is basically unchanged. The nanocomposite residue from the TGA curves increases with

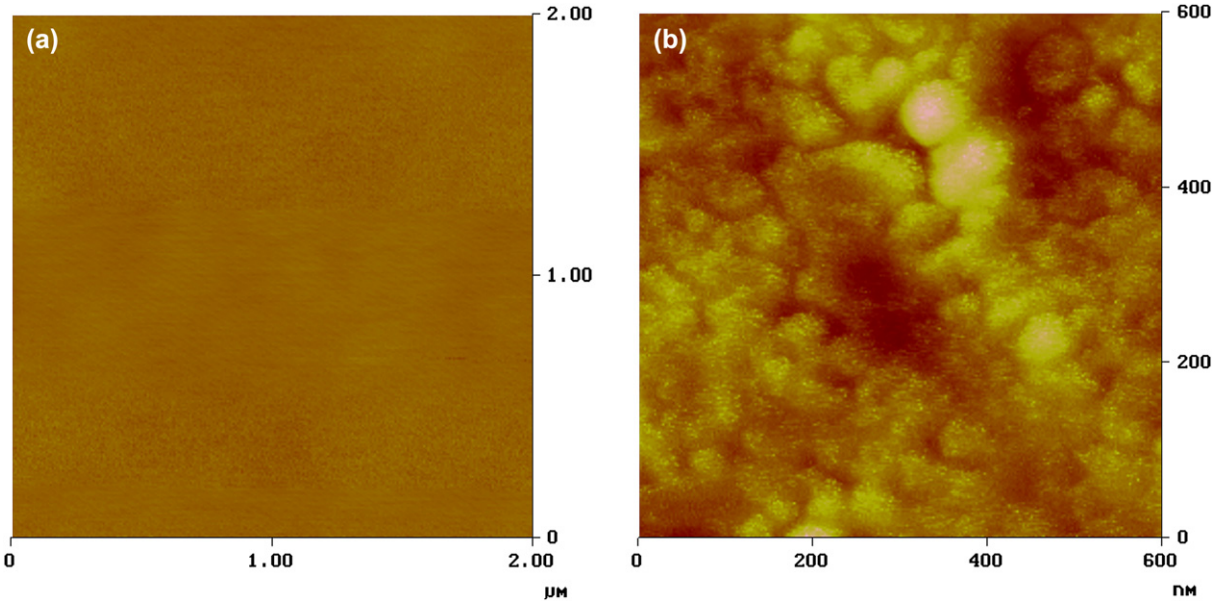

Fig. 6. AFM images of the films (a) without ZnS and (b) with ZnS nanoparticle content of 15 wt%.

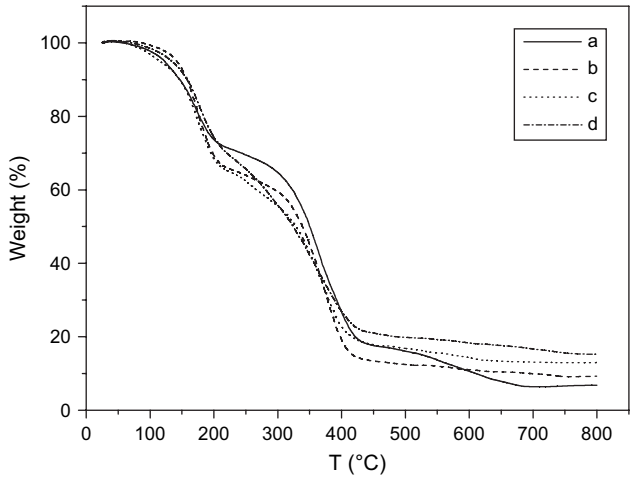

Fig. 8. TGA curves of ZnS/AH20 nanocomposite films with ZnS contents of (a) 5 wt%, (b) 10 wt%, (c) 15 wt%, and (d) 20 wt%.

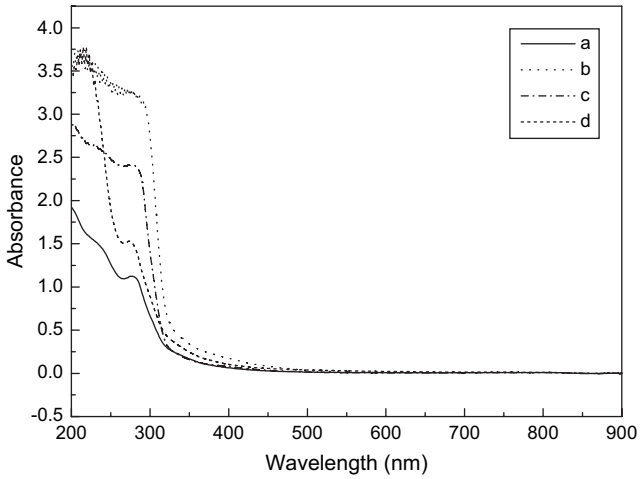

Fig. 10. UV–vis absorption spectra of ZnS/AH20 nanocomposite films with ZnS contents of (a) 5 wt%, (b) 10 wt%, (c) 15 wt%, and (d) 20 wt% on quartz plates.

increasing ZnS content. Moreover, the residue amounts measured is in good accordance with the calculated values of pure ZnS in the nanocomposites.

3.3. Optical property

The optical transparency of ZnS/AH20 nanocomposite films with a thickness of about 1 μm, using a blank quartz plate as the reference, was determined, as shown in Fig. 9. It can be observed that the transmittance of all nanocomposite films with different ZnS contents is over 91% at the wavelength of 500 nm. This result indicates that the ZnS nanoparticles are uniformly distributed in the films, resulting in good optical homogeneity.

The UV–vis absorption spectra of ZnS/AH20 nanocomposite films on a quartz plate with a thickness of about 1 μm was also examined, as shown in Fig. 10. The shoulder peak at around 275 nm for all films appears accompanying a considerable increase in the absorbance. Moreover, with increasing the

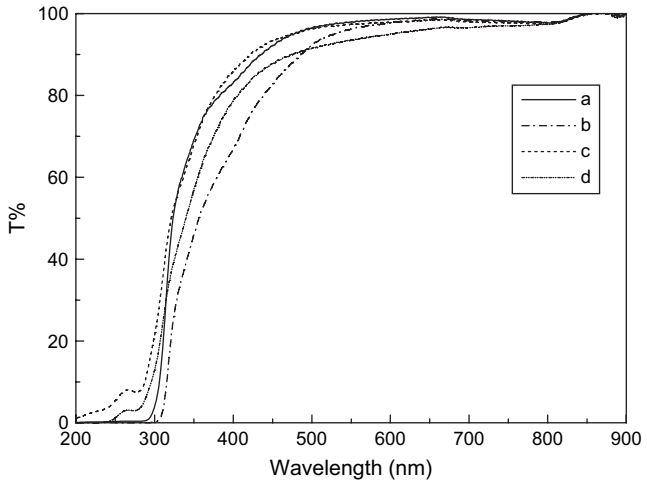

Fig. 9. Optical transmittance spectra of ZnS/AH20 nanocomposite films with ZnS contents of (a) 5 wt%, (b) 10 wt%, (c) 15 wt% and (d) 20 wt%.

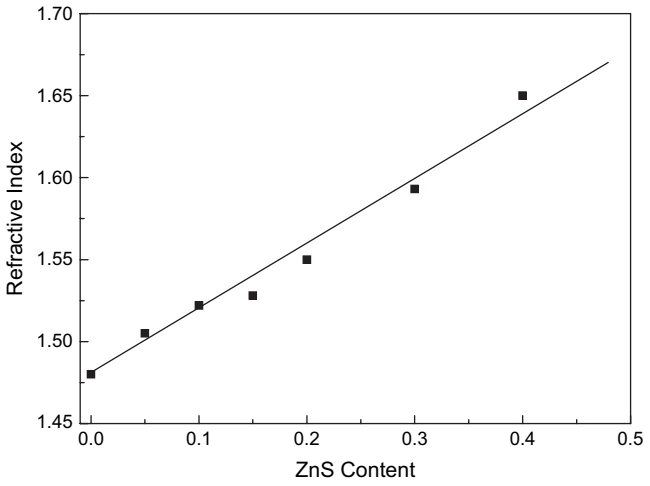

Fig. 11. Refractive index of ZnS/AH20 nanocomposite film as a function of ZnS content.

ZnS content in the nanocomposite film, the overall absorbance increases continuously. These results indicate that the ZnS nanoparticles exhibit a blue shift of absorption onset compared with that of bulk ZnS (335 nm, 3.7 eV) showing a quantum size effect [25].

Fig. 11 shows the change in the refractive indices of nanocomposite films with different ZnS contents. It can be seen that the refractive index of ZnS/AH20 nanocomposite films increases almost linearly with increasing ZnS content. When 40 wt% capped ZnS nanoparticles was introduced into the AH20 matrix, the refractive index of nanocomposite films even reaches up to 1.65. This result indicates that the ZnS nanoparticles contributed significantly to the increase in the refractive index of a nanocomposite film [27].

4. Conclusions

In conclusion, acrylated 2-(2-mercapto-acetoxy)-ethyl ester-capped colloidal ZnS nanoparticles with narrow size

distribution were synthesized. TEM studies suggested that the ZnS nanoparticles uniformly dispersed in the acrylated hyperbranched polyester matrix and remain their original size without aggregation. The high optical homogeneity was obtained with the formed film containing high ZnS content up to 20% by UV–vis spectra. In this system, hyperbranched polyester plays an important role in stabilizing and dispersing ZnS nanoparticles. The technique assisted by this method could be used to prepare various semiconductor nanocomposite films, which possess some potential applications, such as optical coatings, optical waveguides, displays and reflectors, etc.

Acknowledgment

This work is supported by National Natural Science Foundation of China (No. 50233030) and (No. 50633010).

References

[1] Blinov LM, Cipparrone G, Pagliusi P, Lazarec VV, Palto SP. Appl Phys Lett 2006;89:1114.
[2] Mochizuki H, Mizokuro T, Tanigaki N. J Photopolym Sci Technol 2006;19:35.
[3] Cartenuto G, Her YS, Matijevic E. Ind Eng Chem Res 1996;35:2929.
[4] Olshavsky MA, Allcock HR. Macromolecules 1995;28:6188.
[5] Qi Y, Ding J, Day M, Jiang J, Callender CL. Polymer 2006;47:8263.
[6] Kim JH, Koros WJ, Paul DR. Polymer 2006;47:3104.
[7] Lee LH, Chen WC. Chem Mater 2001;13:1137.
[8] Wang B, Wilkes GL. J Polym Sci Part A Polym Chem 1991;29:905.
[9] Papadimitrakopoulos F, Wisniecki P, Bhagwagar DE. Chem Mater 1997;9:2928.
[10] Kypriandou-Leodidou T, Althaus HJ, Wyser Y, Vetter D, Buchler M, Caseri W, et al. J Mater Res 1997;12:2198.
[11] Kypriandou-Leodidou T, Caseri W, Suter UW. J Phys Chem 1994; 98:8992.
[12] Hirai T, Miyamoto M, Komasawa I. J Mater Chem 2000;10:2234.
[13] Hirai T, Watanabe T, Komasawa I. J Phys Chem B 1999;103:10120.
[14] Lu C, Cui Z, Wang Y, Li Z, Guan C, Yang B, et al. J Mater Chem 2003;13:2189.
[15] Jiang G, Wang L, Yu H, Chen C, Dong X, Chen T, et al. Polymer 2006;47:12.
[16] Žagar E, Žigon M, Podzimek S. Polymer 2006;47:166.
[17] Jiang G, Wang L, Chen T, Yu H, Dong X, Chen C. Polymer 2005; 46:9501.
[18] Zou J, Zhao Y, Shi W, Shen X, Nie K. Polym Adv Technol 2005; 16:55.
[19] Hawker CJ, Malström E, Frank CW, Kampf JP. J Am Chem Soc 1997;119:9903.
[20] Zhao Y, Zou J, Shi W. Mater Lett 2005;59:686.
[21] Zhao Y, Zou J, Shi W, Xiang T. Microporous Mesoporous Mater 2006;92:251.
[22] Zhao Y, Zou J, Shi W. Mater Sci Eng B 2005;121:20.
[23] Rauf A, Parveen H. Eur J Lipid Sci Technol 2004;106:97.
[24] Wei H, Kou H, Shi W, Nie K, Shen X. J Coat Technol 2003;75:939.
[25] Zhao Y, Chen T, Zou J, Shi W. J Cryst Growth 2005;275:521.
[26] Hosokawa H, Fujiwara H, Murakoshi K, Wada Y, Yanagida S, Satoh M. J Phys Chem 1996;100:6649.
[27] Lu C, Cheng Y, Liu Y, Liu F, Yang B. Adv Mater 2006;18:1188.